Cooling of a tube by a two-phase flow under microgravity conditions

Tomás Pereira Nave Henriques da Silva
tomas.h.silva@tecnico.ulisboa.pt

Instituto Superior Técnico, Universidade de Lisboa, Portugal

October 2021

Abstract

This report presents a study of the modelling of liquid-vapour flows during the chilldown of rocket engines by a cryogenic fluid in microgravity. A thorough literature review on reduced gravity quenching experiments is presented, showing the scarcity of experimental data and accurate models. Experimental results obtained with the quenching of a stainless steel tube by HFE7100 are presented. The impact of gravity level, flow mass flux and liquid subcooling on film boiling, rewetting temperature, critical heat flux and nucleate boiling is investigated. A correlation for the film boiling regime is presented, validated for HFE7100 and LN2, for terrestrial and microgravity conditions.
Keywords: quenching, microgravity, film boiling, rewetting temperature, critical heat flux, nucleate boiling

1. Introduction

Since the 1960s, cryogenic engines have been used for their high efficiency. This type of engines has been used in Ariane launchers for decades, especially in the upper stages, which means that they are responsible for correctly inserting the payload in orbit.

In particular, Ariane 5 ES (Evolution Storable) is equipped with an upgraded storable propellant stage, allowing re-ignition and long coast phases [9]. Moreover, the upper stage of the upcoming Ariane 6 is powered by the re-ignitable Vinci engine [2]. During the re-ignition phases of the cryogenic engines, it is necessary to chilldown the supply pipes and the turbopumps beforehand. To do so, the cryogenic propellants are injected into the tubes which are at a temperature close to 300K. Since the cryogenic liquids used as fuels in space applications must be free of vapour, being able to predict when a certain tube subjected to a particular set of flow conditions has been sufficiently cooled down, so that the propellant can flow through it without phase-changing, is a critical safety concern.

From a mission point of view, it is important to have an accurate estimation of the time that this chilldown process takes, along with the mass of propellant necessary. Since the liquid used to cool down the tubes is not re-used for combustion purposes, an accurate model of the chilldown process allows to reduce the quantity of propellant wasted.

Moreover, in the future of space activity it will be important to have the capability of refuelling spacecraft in-orbit. This idea has already been studied and some well-thought projects exist in paper, such as the OTV Network System [14]. However, for this to be possible, a good knowledge and understanding of the two-phase flow characteristics of cryogenic fluids is paramount, seeing that the transfer lines between storage tanks would also need to be cooled down.

In both cases, one fundamental aspect that makes the modelling of the chilldown process more complex is the fact that it happens in weightless conditions. In fact, there is very little data in literature regarding two-phase flow heat transfer in microgravity, which is why the work developed presented in this report is useful.

2. Background

The research about flow heat transfer under microgravity conditions started in the 1960's due to the rapid growth of the space industry and the need to understand how fluids behave in low gravity. Initially, the research was mainly focused in the pool boiling mechanisms, but since then a considerable amount of research has also been conducted on flow patterns and flow maps for adiabatic two-phase flow, that made possible the refinement of the boiling models. However, low gravity flow boiling, unlike pool boiling and adiabatic two-phase flow, has not received much attention in the past mainly due to the fact that it is, by far, the more complex of the three phenomena. In addition, thor-

ough understanding of pool boiling is a necessary initial step in analysing flow boiling since it constitutes a fundamental element of the latter.

There are four platforms where microgravity experiments can be performed. The terrestrial-based options include sounding rockets, parabolic flights and drop towers. Then, there is also the possibility of performing the experiments in the International Space Station (ISS).

First, drop towers are the least expensive option, are easy to use and offer the best microgravity levels among the three terrestrial-based options. Moreover, they can be operated on a daily basis and allow the experiment hardware to be changed at short notice and the experiment set-up to be adjusted or improved between drops [10]. However, its use is not suitable for all kinds of experiments since it only offers a few seconds of microgravity per trial (10 seconds maximum), which may not be enough to complete an experiment. On the other hand, parabolic flights are also relatively easy to use and have the advantage of offering longer microgravity periods (around 20 seconds) and allowing the intervention of researchers during the experience. Nevertheless, the cost is higher and the flights need to be booked a few months in advance.

In order to increase the microgravity period to a few minutes, sounding rockets can be used to perform the experiment. Despite this great advantage, the cost is even higher than for parabolic flights and it takes a few years to design and implement the experiment on the rocket. Moreover, once its launched, the researchers have little possibility to intervene. Finally, long weightlessness periods can be obtained by performing the experiments in the ISS. Not only the microgravity level is very low, but the astronauts can intervene in the experiments if necessary. Nevertheless, sending an experiment to the ISS is a very expensive and complex process, which may take years between the experiment design and its implementation. During the experiment, the data are downloaded by telemetry but the payload does not always return to Earth. All in all, the longer the microgravity period, the higher the cost and time required to perform the experiment.

Figure 1 illustrates the typical boiling curve for saturated water, initially plotted by [12], showing the heat flux as a function of the wall superheat, which is the difference in temperature between the wall and the fluid. This curve can be traversed from left to right (heating) or vice-versa (quenching), depending on the relative superheat and the imposed method of wall heat flux. Moreover, it is possible to observe three different boiling regimes, namely: film boiling (FB), transition boiling (TB), and nucleate boiling (NB). These regimes are separated by three critical points, the Leidenfrost Point, LFP (point C), the Critical Heat Flux, CHF (point B), and the onset of nucleate boiling, ONB (point A).

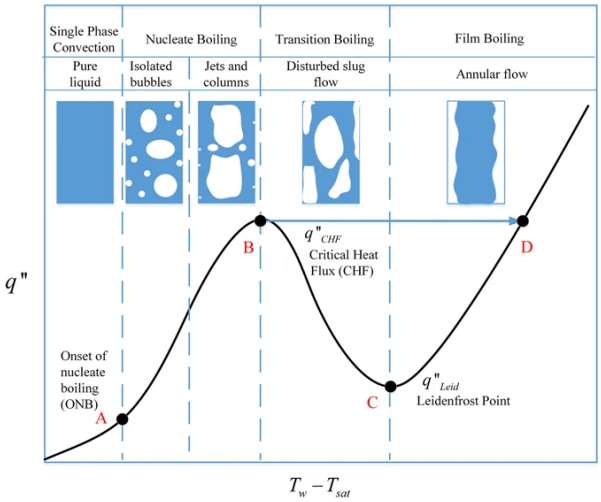

Figure 1: Boiling curve for saturated water.

In the quenching or chilldown configuration, the curve is traversed from right to left. Chilldown begins in the vapour film boiling regime due to the rapid evaporation of the liquid in the immediate vicinity of the wall at high temperature. Depending on the local conditions (inlet pressure, quality, mass flux, and degree of subcooling), the flow will proceed into dispersed flow film boiling (higher quality, low subcooling, and low mass flux) or inverted annular film boiling (IAFB) (low quality, high subcooling, and high mass flux). The latter is the one observed in our case. Film boiling is the least efficient regime regarding the transfer of energy from the wall, for the fact that a film of vapour fully covers its surface, forming an insulating layer due to the low thermal conductivity of vapour, therefore decreasing the heat transfer coefficient.

As the transfer line cools down, the system approaches the LFP, or rewetting temperature, where the heat flux reaches its minimum due to the existence of the insulating vapour layer combined with low wall superheat. The flow then proceeds and passes quickly through TB, characterised by intermittent contact between the liquid and the wall. This regime ends when the liquid is in full contact with the wall, at the point of CHF, where the heat transfer coefficient reaches its maximum value due to the highly efficient cooling process of boiling liquid through use of sensible and latent energy, and since the insulating vapour layer is not present anymore.

Next, the nucleate boiling regime, where heat is generated by vapour bubbles formed in surface cavities that are swept away from the wall surface. As the wall cools further, the system approaches the ONB, defined as the point at which the sys-

tem progresses from nucleate two-phase cooling to single-phase liquid convection. Vapour-free liquid marks the end of the chilldown test.

This boiling curve is similar for the heating and quenching configurations. However, the value of the CHF can largely differ and a strong hysteresis may be observed in the nucleate boiling regime.

3. Experimental apparatus and Procedure

This chapter will present the experimental set-up designed, built and tested in the scope of a PhD thesis [3] by Mr. Brian Verthier and Prof. Dr. Catherine Colin, his supervisor. All the experimental data used in the present report comes from this experiment that took place in 2009, therefore it is interesting to understand its fundamentals.

3.1. Working fluid

The fluid used was the 3M™ Novec™ 7100 Engineered Fluid [1] (HFE7100), which is part of a new generation of refrigerant fluids from the hydrofluoroethers family that are suitable to use in place of older refrigerant fluids such as R113 and R123. The main advantage of this new generation of fluids is the fact they are less harmful for the environment.

This fluid was chosen for its very low surface tension and viscosity, that make it one of the non cryogenic fluids whose physical properties are closest to the ones from liquid oxygen and liquid hydrogen. Furthermore, its low boiling point at 61 °C makes it suitable for boiling experiences. Finally, the other reason for which this fluid was selected was the fact that, for safety reasons during the parabolic flight, it was necessary to use a fluid whose behaviour at high temperatures was known. Incidentally, [15] had already shown in a previous study that the continuous exposition to high temperatures did not generate a dangerous quantity of toxic decomposition products.

3.2. Experimental set-up

As described in [16], the experimental apparatus is a classical two-phase flow loop that can be divided in two main loops:

- The hydraulic one is a closed loop in which the fluid circulates at a given mass flow rate, temperature and pressure.
- The air loop is used to impose the fluid loop pressure. This pressurisation is made by means of a bellows (component Ta1 in the figure 2), which is in contact with air on one side, and with HFE7100 on the other.

The main components of the hydraulic section are shown in figure 2. In the circuit, the refrigerant pressure varies from 0.8 to 2 bar and the liquid subcooling from 5 to 15 °C.

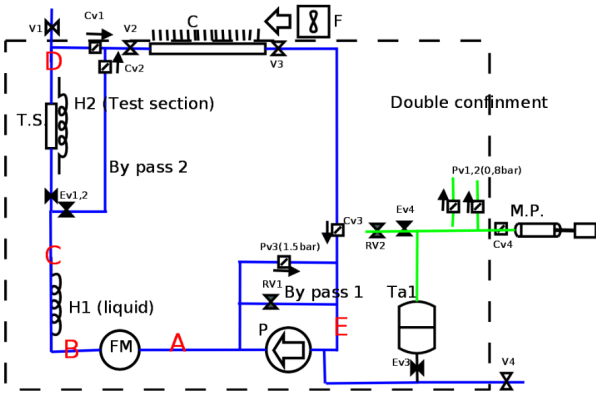

Figure 2: Scheme of the two-phase flow loop used in the experiment.

The hydraulic circuit consists of a main loop, containing the test section (T.S), a condenser (C) to condense the vapor generated during the quenching, a preheater (H1), a pump (P), and two bypass valves (1 & 2). The bypass 1 is used to set up the mass flow rate. The bypass 2 is used to choose if the fluid passes through the test section or not. The branch choice is made by two normally closed electro-valves (Ev 1,2).

The test section is a stainless steel tube, with a 10mm inner diameter, a 1mm thickness and a 10cm length, heated by three resistive heating tapes. 15 k-type thermocouples are attached to the test section outer surface. A k-type thermocouple is inside the test section to measure the liquid temperature. The test section is located between two thermoplastic insulating bridles. In each bridle, two O-ring electrodes are flush-mounted to measure the void fraction from a capacitance method. A k-type thermocouple passes through each bridle to measure inlet and outlet liquid temperatures.

During each parabola, the quenching trial of the test section is divided into 3 phases:

1. Regulation phase: This phase takes place during the five-minute pauses between groups of parabolas, and it is used to modify the global temperature of the circuit. This operation is long and costly in terms of energy consumption, since not only it is necessary to change the temperature of the working fluid, but also the temperature of another components such as the circuit's lines or the pump. During this phase, all the HFE7100 is in the liquid state and circulates via the bypass.

2. Adjustment phase of the test parameters: Two minutes before each quenching trial, the mass flux and the pressure are modified to the desirable values. Simultaneously, the test section is heated and the liquid inside it is vaporised. The vapour generated by the heating of the

test section is evacuated using the one-way valve located after the pyrex tube, and then it is condensed by the condenser.

3. Quenching phase: At the beginning of the microgravity period, the test section is full of vapour and heated to a temperature of 180°C. At the same time, the heating is switched off and the working fluid is deviated from the bypass and starts passing through the branch line containing the test section. This marks the beginning of the quenching. The vapour generated during the trial is evacuated and recondensed. At the end of this phase, the liquid is deviated to the bypass and the second phase starts all over again.

3.3. Metrology

Several physical measures are required to analyse the quenching process, calculate the heat flux and the rewetting temperature. A general scheme of the metrology used is presented in figure 3.

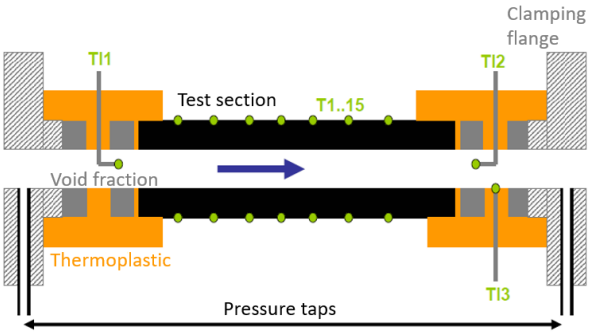

Figure 3: Sensors in the test section.

In order to measure the in-flight acceleration felt by the experimental apparatus, a 3-axis accelerometer is located approximately 20cm from the test section, attached to the frame of the apparatus.

The flow rate is measured by a Coriolis effect flowmeter. This technology was chosen because the fluid being dielectric, the use of an electromagnetic flowmeter was impossible. Likewise, the measure had to not be impacted by the level of gravity.

The absolute pressure is measured upstream of the test section and upstream of the pump, the point where the pressure is imposed. The pressure gradient between the inlet and the outlet of the section is measured between two taps made in the clamps of the latter, using a pressure differential sensor.

The temperature of the liquid phase of the fluid is measured at the inlet and outlet of the test section by two k-type sheathed thermocouples (TI1 and TI2). A third thermocouple TI3 allows to measure the temperature of the thermoplastic's wall. Moreover, the temperature of the test section is measured in 15 positions by unsheathed K-type thermocouples. These were fixed to the wall by a thermosetting resin with a high thermal conductivity, ensuring good mechanical strength and correct thermal contact.

3.4. Data Processing

3.4.1. Heat Flux

In order to obtain the temperature of the wall's inner surface, it is necessary to apply an inverse method. In other words, we measure the temperature of the wall on its external surface, while the cooling takes place on its inner surface. A classical resolution cannot then be applied because the boundary conditions on the inner surface are not known.

We are therefore interested in solving the heat equation using a shooting method. The simplified case of the 1D cylindrical unsteady heat equation (1) was used, where r is the radial direction, varying between D/2 and D/2+e, and φ is the local flux density in W/m^2. It was also assumed that the temperature is invariant with the angle, which is a reasonable assumption given that the test section is vertical.

$$\frac{1}{r}\lambda_w \frac{\partial r\varphi}{\partial r} = \rho_w C p_w \frac{\partial T}{\partial t} \tag{1}$$

By adopting the discretisation shown in figure 4, and by noting T_n^i the temperature of the mesh n at time i and choosing time and space steps dt and dr, the heat equation can be discretised according to equation 2. $F(t)$ is a known function giving the temperature at the internal surface of the wall at time $t = i + 1$ as a function of time $t = i$ according to $T_1^{i+1} = F(i) \times T_1^i$, and $C = (\lambda_w dt)/(\rho_C p_w dr)$.

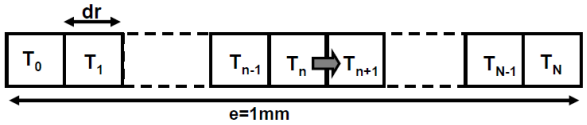

Figure 4: Discretization of the wall in 1D Cartesian for inverse problem solving.

$$\begin{pmatrix} T_1^{i+1} \\ T_2^{i+1} \\ \vdots \\ T_{N-1}^{i+1} \\ T_N^{i+1} \end{pmatrix} = M \times \begin{pmatrix} T_1^{i} \\ T_2^{i} \\ \vdots \\ T_{N-1}^{i} \\ T_N^{i} \end{pmatrix} \tag{2}$$

$$M = \begin{pmatrix} F(i) & 0 & \dots & \dots & \dots & 0 \\ 0 & \frac{C}{2r}+\frac{C}{dr} & 1-2\frac{C}{dr} & \frac{C}{2r}+\frac{C}{dr} & \ddots & \vdots \\ 0 & \ddots & \ddots & \ddots & \ddots & 0 \\ \vdots & \ddots & 0 & \frac{C}{2r}+\frac{C}{dr} & 1-2\frac{C}{dr} & \frac{C}{2r}+\frac{C}{dr} \\ \vdots & \dots & 0 & \frac{C}{2r}+\frac{C}{dr} & 1-2\frac{C}{dr} & \frac{C}{2r}+\frac{C}{dr} \end{pmatrix}$$

Therefore, the method consists of calculating the corresponding external temperature from an internal temperature profile $F(t)$. The error between the calculated and measured profiles is then subtracted from the internal profile, before iterating the calculation. The initial temperature profile chosen corresponds to a stationary 1D profile $T_1 = T_N - e/\lambda_w Q(z,t)$, where the heat flux $Q(z,t)$ is obtained by assuming a uniform wall temperature (equation 3).

$$Q(z,t) \approx \frac{\rho_w A_w C p_w}{P_w} \frac{\partial T_w(z,t)}{\partial t} \tag{3}$$

3.4.2. Rewetting Temperature

The calculation of the rewetting temperature from the experimental data obtained is not straightforward. In fact, the rewetting process is not instantaneous, which means that there is not a well-defined temperature value above which the wall is dry and below which the wall is wet. What happens is that there is a range of temperatures in which there is an intermittent contact between the liquid and the wall, as it was observed by [11] using water and by [17] using liquid nitrogen. This intermittent process is part of the transition regime between the film boiling and the nucleate boiling.

In the plot of the wall temperature as a function of time (figure 6), one can observe that the rewetting phenomenon results in a change of the curve's slope. However, since that change is not instantaneous, the question of where should one consider the rewetting point is raised.

In the literature, different approaches can be found. The first definition by [5] says that the rewetting temperature can be found by the intersection of the curves with the slopes of the film boiling and nucleate boiling regimes. However, implementing this method can be somewhat difficult in our case, due to the fact that the wall temperature does not have a perfectly linear behaviour with time in film and nucleate boiling regimes. As a consequence, depending on whether one considers an averaged slope over the entire regimes, or just a few seconds near the rewetting point, the rewetting temperature value may vary.

Another method used is to consider the temperature at which the maximum temperature variation occurs, which can be easily obtained by taking a second derivative criterion of the maximum temperature. However, it was found by observing figure 5 that it had a slight offset with the actual rewetting temperature value since the point was already in the transition boiling regime. On the contrary, by using the minimum value of the third time-derivative it is possible to obtain the rewetting temperature with great precision. Physically, the minimum of third time-derivative represents the point where the "acceleration" of the temperature reaches a maximum absolute value. In other words, it is the point where the "acceleration" to decrease the temperature is maximal. This makes sense because the flow is shifting from the film boiling regime, where the heat transfer is low, to the transition/nucleate boiling regime where the heat transfer is much higher, causing a big variation of the temperature's variation velocity.

To conclude, it appears that the third time-derivative based definition is the most robust and the most objective, since it does not involve an arbitrary criterion on the smoothing interval. It can be obtained simply by considering the third time-derivative of the temperature and it is then subject to fewer calculation errors. Therefore, this is the definition of rewetting temperature that was used in this work.

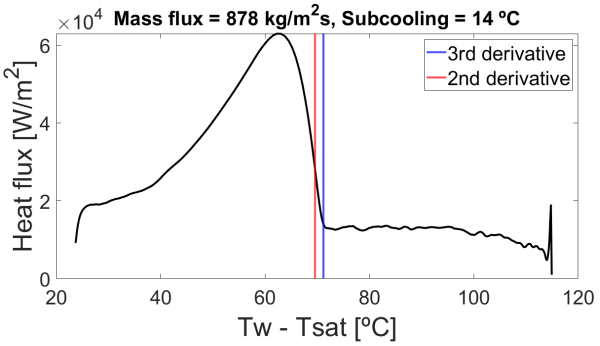

Figure 5: Comparison of methods to find the rewetting temperature.

3.4.3. Rewetting Velocity

In order to calculate the rewetting velocity, the time difference between the rewetting point of two thermocouples was used. Ideally, this could be done using all 12 thermocouples available in order to access the evolution of the rewetting velocity along the wall. However, this was not possible due to the fact that the temperature of the wall is not uniform along the tube due to the experimental conditions. If we consider that, for the same operating conditions, two points have an equal rewetting temperature, it would not be correct to compare points with a different initial temperature because the point with the higher temperature would take longer to reach the rewetting temperature and that time difference would induce an error in the rewetting velocity measurement. Hence, the only solution was to find thermocouples with a close initial temperature and that had a well-defined film boiling regime.

The pair of thermocouples that better check this requirements is formed by thermocouples 7 and 9 (T7 and T9), located 6cm and 7cm from the inlet, respectively. Both thermocouples have an initial temperature between the 170 and 180 ºC in all

the experiment trials. The rewetting velocity is then calculated by dividing the distance between T7 and T9 by the time difference between the rewetting instant in those two thermocouples (figure 6). Furthermore, a selection of the trials was made in order to obtain results as close to reality as possible. This selection was based in two criteria: initial temperature difference between T7 and T9; and rewetting temperature difference between T7 and T9. For both parameters, the maximum difference allowed was 3ºC. As a result, the selection is comprised of 20 trials in microgravity and 34 trials in normal gravity.

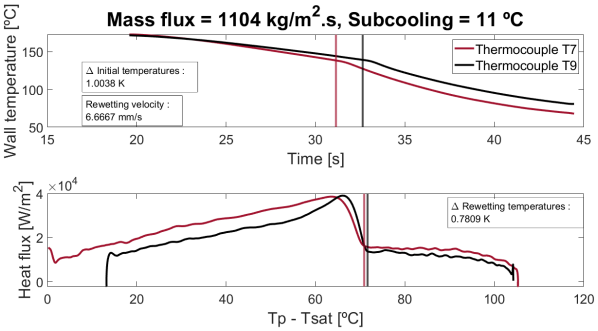

Figure 6: Computation of the rewetting velocity.

4. Results & discussion

4.1. Thermocouple used and reference points

Experimentally, the boiling curve can be very different depending on the thermocouple from which the data is obtained. It is very difficult to have perfect experiment conditions and the thermocouples have different initial temperatures. This factor combined with the different positions of thermocouples along the tube results in the different boiling curves. Having said that, to perform our analysis it was necessary to decide which thermocouple we would use. Looking at figure 7 not only for the shown example but for all trials, it was decided the thermocouple 8 (T8) was the best since its boiling curve is very well-defined in all the trials (well-marked film boiling with constant heat flux, clear rewetting point, transition boiling and nucleate boiling regimes in accordance to the theoretical model and a distinct peak corresponding to the critical heat flux) and it has an approximately constant initial temperature as well. Therefore, all the results presented from now on were obtained with data from T8, except for the rewetting velocity which was calculated with T7 and T9, as explained previously.

In order to characterise the heat exchange coefficients in the different boiling regimes, certain characteristic points of the boiling curve were chosen. These points are used to analyse the relative influence of each parameter on the different boiling regimes as well as for the comparison of measurements with models and correlations in the literature.

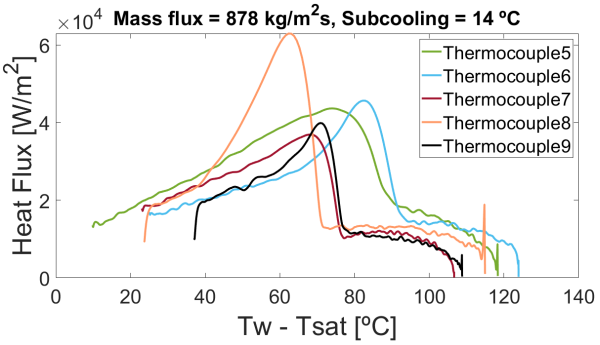

Figure 7: Boiling curve of different thermocouples.

Figure 8 shows the selected points. Going through the boiling curve from the right to the left, i.e., from the highest superheats to the lowest, one can observe the film boiling point at a superheat of 90ºC, followed by the rewetting point and the critical heat flux point. Finally, there is the nucleate boiling point at a superheat of 55ºC.

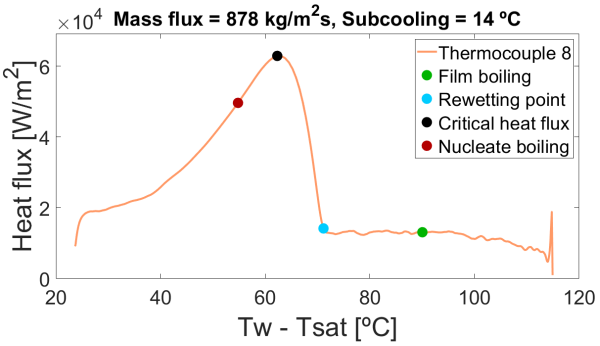

Figure 8: Location of the reference points in the boiling curve.

4.2. Qualitative results

In terms of qualitative results, it is possible to conclude that the increase of flow mass flux and liquid subcooling lead to an increase in the heat flux in all the regimes/critical-points except for the nucleate boiling regime, where this is not verified under microgravity conditions due to the dominance of the nucleate boiling mechanism over the forced convection. In terms of gravity levels, a significant decrease of the heat flux in the film boiling regime was found in microgravity, especially for lower mass fluxes. For higher mass fluxes, the difference in the heat flux gradually decreases. Moreover, the rewetting velocity is reduced to almost one half under microgravity conditions. In the other regimes, the influence of gravity is not clearly pointed out.

4.3. Modelling of the film boiling regime

Since film boiling is the regime that takes more time to complete, it is the one that influences the most

the total time of the quenching process. Therefore, an accurate prediction of this regime would come a long way in the correct modelling of the boiling curve.

Hence, a simple analytical model was developed for the film boiling regime by assuming a quadratic velocity profile for the vapour layer (figure 9) and the following boundary conditions:

$$u_v|_{y=0} = 0 \tag{4}$$

$$u_v|_{y=\delta} = u_i \tag{5}$$

$$\upsilon_v\left(\frac{\partial^2 u_v}{\partial y^2}\right) = -\left(\frac{\rho_l}{\rho_v} - 1\right) g \tag{6}$$

For simplification purposes, the thermal boundary layer and the boundary layer between the vapour and liquid phases were neglected. Moreover, the vapour velocity at the interface was assumed equal to the velocity of the liquid, i.e., $u_i = u_L$. Furthermore, the temperature profile, the mass flux balance and the enthalpy balance are given by equations 7, 8 and 9, respectively. This approach consists in doing what [4] did for the case of an upward flow forced convection film boiling from the outside of a horizontal tube, but applied to a flow over a flat plate. Despite the simplicity of this model, it was not found in the literature review.

$$T = T_p + (T_{sat} - T_p)\frac{y}{\delta} \tag{7}$$

$$\dot{m} = \rho_v \overline{u_v} b\delta = \frac{\rho_v b u_L \delta}{2} + (\rho_l - \rho_v)\frac{bg\delta^3}{12\upsilon_v} \tag{8}$$

$$dq = h\Delta T dA = \frac{\lambda_v}{\delta}\Delta T b dx = d\dot{m} h^*_{lv} \Leftrightarrow \delta = \frac{\lambda_v b \Delta T}{h^*_{lv}\left(\frac{d\dot{m}}{dx}\right)} \tag{9}$$

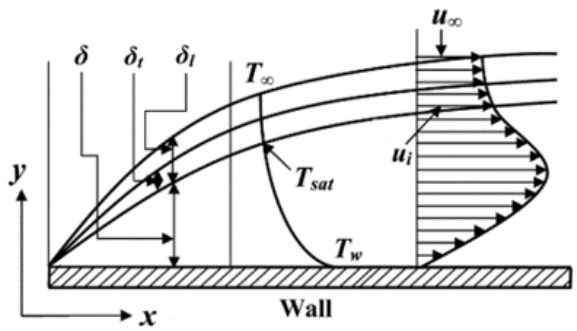

Figure 9: Schematic of the flow over the flat plate.

After developing these equations, one can obtain the final expression for the heat transfer coefficient in the film boiling (equation 10). This coefficient is calculated as an average in the region between the rewetting point and a point upstream in the tube located at a characteristic length L_{ref}.

$$h = \frac{4}{3\sqrt{3}}\sqrt{\frac{u_L \lambda_v \rho_v h^*_{lv}}{L_{ref}\Delta T}}\cdot\left[1 + \sqrt{1 + \frac{9}{16}\frac{\lambda_v(\rho_l - \rho_v) g L_{ref}\Delta T}{u_L^2 \rho_v \mu_v h^*_{lv}}}\right]^{1/2} \tag{10}$$

Figures 10 and 11 shows the results predicted by the proposed model for both gravity levels. The value of L_{ref} was adjusted for each gravity level in order to better match the experimental results, and the results presented were obtained with $L_{ref} = 0.036m$ in normal gravity and $L_{ref} = 0.012m$ in microgravity. Using these values, one can observe that the results obtained in microgravity conditions compare well with the experimental data, since the trend lines are superposed. In microgravity, the increase in heat flux for higher masses is also correctly predicted, but the heat flux is underestimated by 10%.

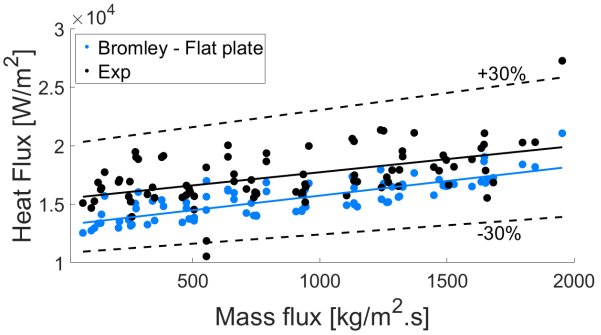

Figure 10: Comparison of the experimental results and the ones predicted by the proposed model, in normal gravity.

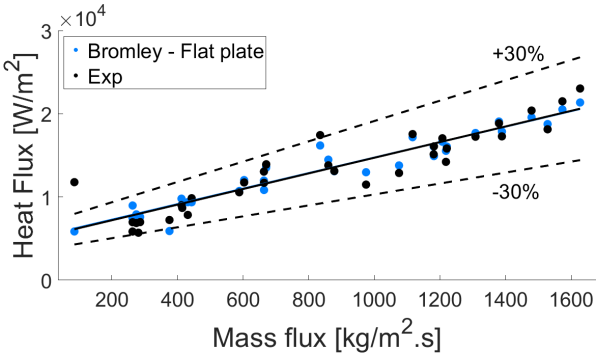

Figure 11: Comparison of the experimental results and the ones predicted by the proposed model, in microgravity.

4.3.1. Validation of the reference length

In order to assess if the values of L_{ref} were in agreement with the physical meaning given to L_{ref}, the rewetting velocity was multiplied by the time difference (Δt) between a superheat of 90ºC or 80ºC and the rewetting point. This was done both in normal gravity and microgravity conditions, and the results are presented in figures 12 and 13. Firstly, it is possible to observe that the order of magnitude of L_{ref} is correct. Secondly, the data for

a superheat of 90 ºC is close to the value of L_{ref} in normal gravity, but in microgravity the value of L_{ref} is between the data for a superheat of 90 ºC and 80 ºC. All in all, these results seem to corroborate the meaning proposed for L_{ref}.

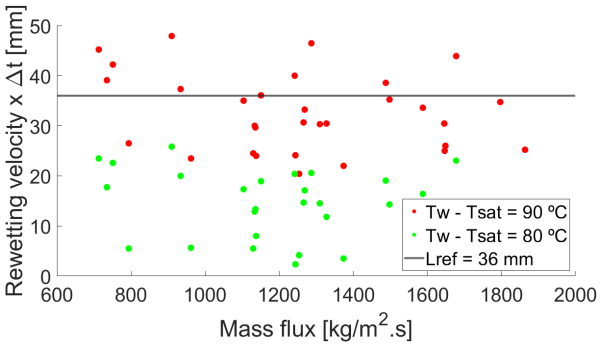

Figure 12: Comparison of the experimental results and the ones predicted by the proposed model, in microgravity.

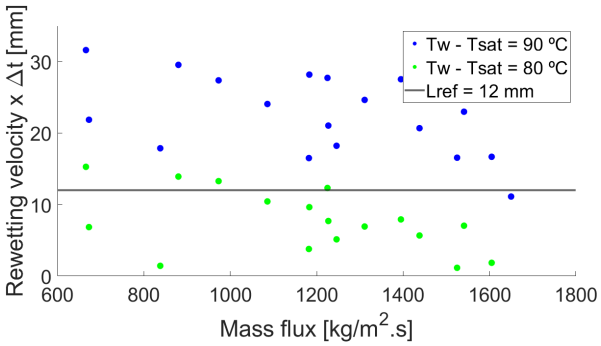

Figure 13: Comparison of the experimental results and the ones predicted by the proposed model, in microgravity.

4.4. Application of the film boiling model to cryogenic fluids

Considering the accuracy obtained with the Bromley-flat plate formula in predicting the heat flux for our experiments, it was decided to test it against the results of the cryogenic experiments made by [6]. Before presenting the results obtained, a few introductory notes are necessary.

First of all, the data from the experiments in terrestrial conditions was not made available by [6], therefore the Bromley-flat plate model was only validated for the microgravity conditions. Secondly, the properties of saturated nitrogen, either in gaseous or liquid state, were obtained in the website [13]. It was not possible to find the source of the information nor its level of accuracy, hence it can be a source of error in the heat flux calculation. Furthermore, it was not possible to find the properties of the material of the tube, 304 stainless steel, in the range of cryogenic temperatures of the experiment. Therefore the properties used are the ones for the range of 0 to 100ºC, and were obtained in the website [8]. The quantitative impact that this approximation has on the obtained results is unknown. Moreover, only four out of the ten trials available were used because the other six had lower mass fluxes and as result did not arrive near the rewetting point before the end of the microgravity period. Hence, either the validation was made for superheats above 100 K using the other 6 trials, or for lower superheats using these 4 trials. It was not possible to do the validation using higher superheats using all the trials because these 4 that were selected were in transitory conditions for those values of superheat. Finally, the L_{ref} value used is exactly the same that was used for the HFE7100 experiments, i.e. no modifications were made in the formula to account for cryogenic fluids.

The comparison between the results obtained and the experimental data can be seen in figure 14, along with best-fit lines for both sets of data. The results are presented for a superheat of 85 K, and it can be observed that the estimation error is inferior to 30% for the entire range of mass flux.

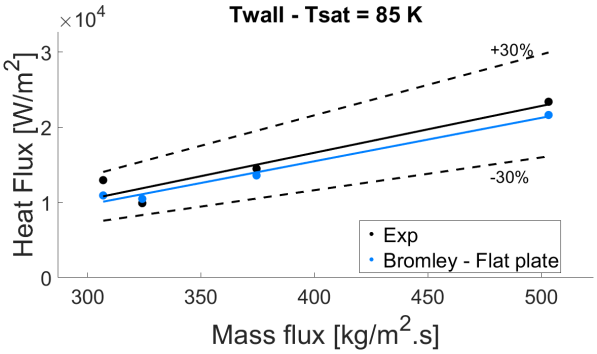

Figure 14: Comparison of proposed model with the cryogenic experimental results.

4.5. Prediction of the variation of the wall temperature with time

Considering the previously presented good results, the question arose as to whether the model was capable of predicting the evolution of the wall's temperature as a function of time, which implicates an accurate prediction of the heat flux throughout the whole film boiling regime.

Figure 15 allows to compare the predicted and the experimental evolution of the wall's temperature with time, for an experiment using HFE7100 and under microgravity conditions. As it is possible to observe, the temperature of the wall decreases 20 ºC over 6 seconds, and the predicted curve exactly matches the experimental one. This is indicative of a correct estimation of the heat flux over the entire range of superheats.

Figure 16 shows the evolution of the wall's temperature for the cryogenic trial with the higher mass flux and, after an initial transitory regime that last around 3 seconds, there are 5 seconds during

which the slope is approximately constant. This is our region of interest since it represents the film boiling regime, and it can be seen that the Bromley-flat plate model predicts the evolution of the temperature with accuracy. In fact, those 5 seconds, the wall temperature decreases more than 40 K, and at the rewetting point there is only a difference of 1.5 K between the predicted temperature and the experimental data. Nevertheless, the prediction is not perfect since the slope of the predicted curve is less pronounced than the experimental one for higher temperatures, then the two curves intersect and closer to the rewetting point the slope of the predicted curve is steeper than the experimental one. This indicates that the heat flux is slightly under-predicted for higher superheats and slightly over-predicted for lower superheats.

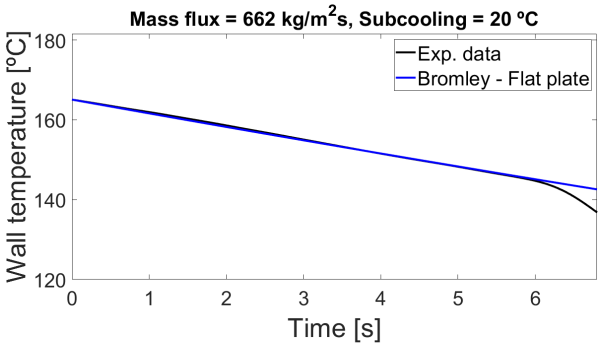

Figure 15: Comparison of the predicted and experimental variation of wall temperature with time, for the HFE7100.

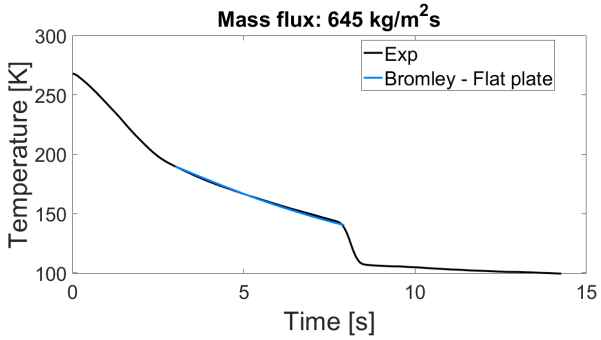

Figure 16: Comparison of the predicted and experimental variation of wall temperature with time, for the LN2.

5. Conclusions

The objective of this internship was to study the modelling of the different boiling regimes during the chilldown of rocket engines by a cryogenic fluid in microgravity. In particular, special focus was given to the theoretical modelling of the film boiling regime, since it is the regime that impacts the most the duration of the chilling process. Hence, a theoretical model coupled with the heat transfers in the tube wall was developed and validated using the data obtained in the scope of the PhD thesis of [3], who designed and built at IMFT an experiment to study the quenching of a stainless steel tube by HFE7100. Furthermore, the proposed model was also validated for cryogenic fluids, using the LN2 data from [7]. For both type of fluids, the correlation is able to predict the heat flux within an error margin always inferior to 30%.

In terms of qualitative results, it is possible to conclude that the increase of flow mass flux and subcooling lead to an increase in the heat flux in all the regimes except for the nucleate boiling regime, where this is not verified under microgravity conditions due to the dominance of the nucleate boiling mechanism over the forced convection. In terms of gravity levels, a significant decrease of the heat flux in the film boiling regime was found, especially for lower mass fluxes. For higher mass fluxes, the difference in the heat flux gradually decreases. Moreover, the rewetting velocity is reduced to almost half under microgravity conditions. In the other regimes, the influence of gravity is not well-defined.

From the bibliographic review made, we can conclude that our findings are in agreement with the majority of the results reported. However, considering that some articles report results contrary to what we found, namely regarding the rewetting velocity, in the future it would be advisable to conduct more experiments to increase the data set and consolidate the results obtained in the chilldown process under microgravity conditions.

Future work should also be focused on doing more experiments of chilldown in microgravity but with an experimental set-up that allowed the visualisation of the wall in order to understand better the physical mechanisms. This is important for the rewetting temperature and critical heat flux points since the present models were developed for the heating configuration and fail to explain what happens during chilldown.

References

[1] (3M™). 3m™ novec™ 7100 engineered fluid. Brochure. `https://multimedia.3m.com/mws/media/1998180/3m-novec-7100-engineered-fluid.pdf`.

[2] A. (ArianeGroup). Ariane 6. https://www.arianespace.com/vehicle/ariane-6/.

[3] Brian Verthier. *Une étude sur les transferts associés aux écoulements diphasiaues de fluides cryogéniques en microgravité : application à la mise en froid de moteurs-fusée*. PhD thesis, Institut National Polytechnique de Toulouse, 2010.

[4] L. A. Bromley, N. R. Leroy, and J. A. Robbers. Heat transfer in forced convection film boil-

ing. *Industrial and Engineering Chemistry.*, 45(12):2639–2646, 1953.

[5] W. J. Chen, Y.Lee, and D. C. Groeneveld. Measurement of boiling curves during rewetting of a hot circular duct. *International Journal of Heat and Mass Transfer*, 22(6), 1979. doi.org/10.1016/0017-9310(79)90039-5.

[6] S. Darr, J. Dong, N. Glikin, J. Hartwig, A. Majumdar, A. Leclair, and J. Chung. The effect of reduced gravity on cryogenic nitrogen boiling and pipe chilldown. *npj Microgravity*, 2(16033), 2016. https://doi.org/10.1038/npjmgrav.2016.33.

[7] S. R. Darr, J. W. Hartwig, J. Dong, H. Wang, A. K. Majumdar, A. C. LeClair, and J. N. Chung. Two-phase pipe quenching correlations for liquid nitrogen and liquid hydrogen. *Journal of Heat Transfer*, 141(4): 042901, April 2019. doi.org/10.1115/1.4041830.

[8] M. M. P. Data". "304 stainless steel". `matweb.com/search/DataSheet.aspx?MatGUID=abc4415b0f8b490387e3c922237098da&ckck=1`.

[9] E. S. A. (ESA). Ariane 5 es. `https://www.esa.int/Enabling\_Support/Space\_Transportation/Launch\_vehicles/Ariane\_5\_ES`.

[10] E. S. A. (ESA). Microgravity and drop towers. `www.esa.int/Education/Microgravity\_and\_drop\_towers`.

[11] M. Ilyas, C. Hale, S. Walker, and G. Hewitt. Rewetting of heated surfaces by intermittently bursting liquid-metal contacts - an experimental study. 7th International Conference on Multiphase Flow, 2010.

[12] S. Nukiyama. Maximum and minimum values of heat transmitted from metal to boiling water under atmospheric pressure. *Journal of the Japanese Society of Mechanical Engineers.*, 37:367, 1934.

[13] "(peace software)". "online calculation of thermodynamic properties of nitrogen". `www.peacesoftware.de/einigewerte/einigewerte_e.html`.

[14] T. Tanabe, S. Nakasuka, and T. Iwata. System and operation analyses of OTV Network - A new space transportation concept. In *15th International Symposium on Space Technology and Science*, volume 2, pages 1475–1480, Jan. 1986.

[15] P. Tuma and L. Tousignant. Experimental study of the decomposition of hfe-7100 vapor in a billet of ti-6al-4v during bakeout at 275℃. 3M internal report, August 2000.

[16] B. Verthier and C. Colin. Heat transfer coefficient and rewetting temperature during the quenching of a tube by hfe7100. 7th International Conference on Multiphase Flow, 2010.

[17] K. Yuan, Y. Ji, and J. N. Chung. Cryogenic chilldown process under low flow rates. *International Journal of Heat and Mass Transfer*, 50(19-20), 2007. doi.org/10.1016/j.ijheatmasstransfer.2007.01.034.